MICROMACHINED STIMULATING ELECTRODES

Quarterly Report #5

(Contract NIH-NINDS-N01-NS-5-2335)

October 1996 --- December 1996

Submitted to the

Neural Prosthesis Program
National Institute of Neurological Disorders and Stroke
National Institutes of Health

by the

Center for Integrated Sensors and Circuits
Department of Electrical Engineering and Computer Science
University of Michigan
Ann Arbor, Michigan
48109-2122

January 1997

This QPR is being sent to you before it has been reviewed by the staff of the Neural Prosthesis Program.

MICROMACHINED STIMULATING ELECTRODES

Summary

During the past quarter, we have continued to fabricate passive stimulating probes and have also realized probes in cooperation with an external foundry (MCNC, Research Triangle Park, NC). The foundry probes use low-stress silicon nitride dielectrics and appear quite acceptable in terms of built-in shank stress, in-vitro tests, and general yield. In-vivo tests are planned during the coming term. We are also beginning work to evaluate the use of TiN layers as an alternative to IrO on some of our stimulating probes. This material does not etch excessively in EDP and is thus compatible with our overall process. It has been reported to have a charge delivery capability significantly better than IrO. We have been using it experimentally under titanium to enhance our circuit contacts, and it is widely known as a passive interdiffusion barrier for contacts in the integrated circuit industry. Probe fabrication using TiN sites will take place during the coming term along with in-vitro and in-vivo evaluation.

We have also begun experiments with parylene as a coating material for some of our stimulating probes. Test probes with parylene coatings 3, 6, 9, and 12μm-thick have been fabricated and the sites have then been laser ablated in cooperation with PI Medical. Some of the sites were subsequently cleaned electrochemically. The impedances of the sites, activated and unactivated, were dependent on the thickness of the parylene and it is expected that a thin layer of parylene was still present on portions of the metal surfaces after ablation. Use of a post-ablation oxygen plasma to remove the residual parylene will be explored during the coming term.

The design of a four-channel 64-site active stimulating probe has now been completed. This probe has been fully simulated and is functional at clock rates exceeding 10MHz. The circuit layout area is 5.7mm^2. The probe allows each of four externally generated stimulus currents to be routed to 16 sites, with one of the sites on each of the 16 shanks. Any of the selected sites can be used for either recording or stimulation. Fabrication of these probes will also take place during the coming term.

MICROMACHINED STIMULATING ELECTRODES

1. Introduction

The goal of this research is the development of active multichannel arrays of stimulating electrodes suitable for studies of neural information processing at the cellular level and for a variety of closed-loop neural prostheses. The probes should be able to enter neural tissue with minimal disturbance to the neural networks there and deliver highly-controlled (spatially and temporally) charge waveforms to the tissue on a chronic basis. The probes consist of several thin-film conductors supported on a micromachined silicon substrate and insulated from it and from the surrounding electrolyte by silicon dioxide and silicon nitride dielectric films. The stimulating sites are activated iridium, defined photolithographically using a lift-off process. Passive probes having a variety of site sizes and shank configurations have been fabricated successfully and distributed to a number of research organizations nationally for evaluation in many different research preparations. For chronic use, the biggest problem associated with these passive probes concerns their leads, which must interface the probe to the outside world. Even using silicon-substrate ribbon cables, the number of allowable interconnects is necessarily limited, and yet a great many stimulating sites are ultimately desirable in order to achieve high spatial localization of the stimulus currents.

The integration of signal processing electronics on the rear of the probe substrate (creating an "active" probe) allows the use of serial digital input data which can be demultiplexed on the probe to provide access to a large number of stimulating sites. Our goal in this area has been to develop a family of active probes capable of chronic implantation in tissue. For such probes, the digital input data must be translated on the probe into per-channel current amplitudes which are then applied to the tissue through the sites. Such probes generally require five external leads, virtually independent of the number of sites used. As discussed in our previous reports, we are now developing a series of active probes containing CMOS signal processing electronics. Two of these probes are slightly redesigned versions of an earlier first-generation set of designs and are designated as STIM-1A and STIM-1B. A third probe, STIM-2, is a second-generation version of our high-end first-generation design, STIM-1. All three probes provide 8-bit resolution in setting the per-channel current amplitudes. STIM-1A and -1B offer a biphasic range using ±5V supplies from 0μA to ±254μA with a resolution of 2μA, while STIM-2 has a range from 0 to ±127μA with a resolution of 1μA. STIM-2 offers the ability to select 8 of 64 electrode sites and to drive these sites independently and in parallel, while -1A allows only 2 of 16 sites to be active at a time (bipolar operation). STIM-1B is a monopolar probe, which allows the user to guide an externally-provided current to any one of 16 sites as selected by the digital input address. The high-end STIM-2 contains provisions for numerous safety checks and for features such as remote impedance testing in addition to its normal operating modes. It also offers the option of being able to record from any one of the selected sites in addition to stimulation. A new probe, STIM-2B, is currently being added to this set. It offers 64-site capability with off-chip generation of the stimulus currents on four separate channels.

During the past quarter, we have continued to fabricate passive probe structures for internal and external users. Passive probes fabricated at MCNC have been etched out successfully and appear acceptable in all respects. Investigations of TiN as a material for stimulating sites (in place of IrO) has also begun. Parylene has been used as an outer

coating on stimulating probes and is being laser ablated over the sites. Finally, the design of STIM-2B has been completed. The results in each of these areas are described more fully in the sections below.

2. *Passive Probe Fabrication*

Our Center for Neural Communication Technology continues to supply passive probes to external users. As described in the last report, these probes are being processed by UM Solid State Electronics Lab staff and, more recently, by an external silicon foundry (MCNC, Research Triangle Park, NC). Wafers fabricated in our lab came from mask sets HMRI, HIDENS, CNCT2 and CNCT3. MCNC fabricated wafers from EMORY and CNCT1. While our laboratory has been producing better quality probes with fewer problems recently, yield and turnaround time continue to be areas where further improvement is needed. In-house fabrication is complicated by the number of users and the range of processes run on all of our process tools. The MCNC foundry has a very restricted group of processes and users, both of which tend to increase the yield and consistency of the devices produced.

MCNC does not perform the entire passive probe process. The deep and shallow diffusions are performed in our Laboratory and a layer of silicon dioxide is deposited for stress compensation. The wafers are shipped to MCNC for dielectrics, polysilicon, and the gold bonding pads. The wafers are then returned to us for deposition of the iridium sites and the final EDP etch. MCNC does not have the same CVD oxide capabilities as our laboratory. The top dielectric is therefore not the SiO_2-Si_3N_4-SiO_2 stack which we typically use, but rather is a single layer of low stress (silicon-rich) nitride. The stress characteristics of the first run of MCNC probes are quite good. There are some other implications, however, to using nitride alone as a dielectric. First, silicon nitride by itself has been shown by David Edell, MIT, (see "Insulating Biomaterials" quarterly reports) to be unreliable as a dielectric material when directly exposed to saline. He has observed much better characteristics with oxide/nitride/oxide composite structures such as those used in our standard process. While thick layers (1μm or greater) of low-stress nitride by itself may be quite sufficient for shorter-term chronic applications and certainly for acute studies, longer term applications such as neural prostheses will most likely require a top layer of oxide or another surface coating such as silicone or a fluoropolymer to guard against dissolution. Since the layers of low-stress nitride MCNC is using are not stoichiometric, it is not clear how leakage measurements performed on other nitride films may translate to this material. Certainly, such leakage is process dependent, and if these films are used on a continuing basis, then appropriate measurements will have to be performed.

Another issue brought about by the MCNC probes is an increase in shunt capacitance due to the modified dielectric structure. Low-stress nitride has a dielectric constant that is about 50% higher than that realized with our composite dielectric structure. Thus, if similar total dielectric thicknesses are used (about 1μm top and 1μm bottom), the shunt capacitance to the surrounding tissue for the MCNC probes may be as high as twice that of our standard probes. As above, an added oxide layer would help minimize this problem.

We intend to study these issues further through soak testing and *in vitro* and through *in vivo* recording sessions in which we will compare signal quality between probes processed in our laboratory and the MCNC probes. In the meantime, we are working on a new mask layout which will be made up of general-use probes for the next MCNC run. Input is being solicited from our probe users on design features and it is

hoped that most needs can be met with a minimal number of designs. The new mask set will be sent to MCNC for fabrication to produce a large inventory of these designs which will make up the new Center catalog. We will still accept custom designs, although it is hoped that the number of required custom runs can be minimized. Custom design masks will still be fabricated in the Michigan Solid-State Fabrication Facility.

While the monolithic silicon cable remains the best option for flexible interconnection to the probes, we are also looking into alternative methods to connect between probes and platforms and the percutaneous connector. This is due to several factors. First, the silicon cables required by many of our external users are often very long (2 to 3cm) and this greatly decreases the number of probes that can be realized on a given wafer. The yield of long cables is also less than we would desire. Second, the silicon cables are fragile and many users have difficulty handling them without breakage. The silicon cable performs best where extreme flexibility is needed for a short distance, such as is required where the probe exits the brain. As the cable exits the subdural space, however, the extreme flexibility afforded by the silicon cable is less critical, and robustness is often a more desirable feature at this point.

One technique being explored is shown in Fig. 1. Parts of this technique were suggested by Gyorgy Buzsaki of Rutgers University. It involves the use of a Kapton-based flexible circuit board for the main interconnect to the probe. These flexible boards consist of copper traces sandwiched between polyimide (typically 1/2 mil) and adhesive layers of epoxy or acrylic. A short length of silicon cable (<1cm) carries signals from the probe to the subdural space. The backend of the silicon cable will be ultrasonically bonded to the flex circuit which will take the signals from the subdural space, through the skull and to the percutaneous connector. Connections between the probe and the Kapton cable will be potted with silicone or perhaps with the fluoropolymers being studied at MIT. While this hybrid technique is similar to the polyimide microribbon technology explored by our group in 1988/89, it relies upon larger-scale flex circuits fabricated by a vendor. Many companies are now capable of etching copper traces on 150μm centers, permitting us to make 16-lead cables as narrow as 2.5mm.

While we are not abandoning the use of the silicon cable as the main interconnect (especially for very long-term implants), the hybrid approach has several advantages, especially for probe distribution. A more robust cable should result in fewer failures due to breakage during surgical handling. There will also be a large increase in probe yield since the silicon portion of the assembly is reduced in size. It will also permit us to utilize the same probe design for either acute or chronic use; since the silicon cable will be relatively short, the cable portion of the probe can simply be mounted further up on our standard rigid PC board for acute use.

3. *Investigation of an Alternative Electrode Site Material*

A paper was published at the IEEE Engineering in Medicine and Biology Society (EMBS) conference in November, 1996, which presented titanium nitride (TiN) as a material to be used in the fabrication of thin film microelectrodes[1]. The authors compared several mechanical and electrical properties of TiN electrodes to those of iridium oxide

[1]M. Janders, U. Egert, M. Stelzle, W. Nisch, "Novel Thin-Film Titanium Nitride Microelectrodes with Excellent Charge Transfer Capability for Cell Stimulation and Sensing Applications," *Digest EMBS*, Amsterdam, November 1996.

(IrO) electrodes. Their results indicate that, despite a lower charge capacity (Q_{cap}), TiN electrodes demonstrate a generally lower impedance (Z) and a significantly higher charge injection capability (Q_{inj}) when compared with IrO electrodes. A quantitative description of these results appears in Table 1. The charge injection capability is a critical characteristic to consider in a material being used for biological electrodes since it is a measure of the amount of charge which that material can inject into tissue without a safe potential range being exceeded. The authors also noted that iridium tends to crack during oxidation, while TiN does not present this problem.

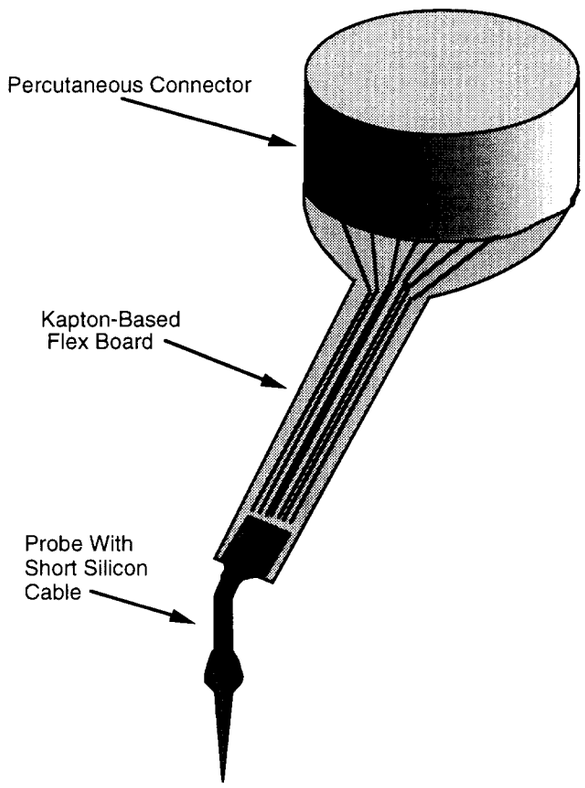

Fig. 1: Schematic of a proposed new chronic assembly. This method utilizes a hybrid approach with a Kapton flex circuit providing the more lengthy connection to the percutaneous connector.

	Q_{inj} (mC/cm^2)	Q_{cap} (mC/cm^2)	$Z_{f=1kHz}$ (kW)
IrO	3.8 - 6.5	up to 240	100 - 750
TiN	23	42	150

Table 1: Electrical properties of IrO and TiN electrodes; electrode areas were $80mm^2$.

We have begun to investigate for ourselves the properties of TiN electrodes, their compatibility with our probe fabrication process, and their possible benefits as an alternative site material for use in stimulating and recording neural probes. The first step in this investigation has been to evaluate the compatibility of TiN with etching in EDP, which is used as the final micromachining step in the Michigan probe process to free probes from the surrounding wafer substrate. TiN was found to etch in EDP at a rate of approximately 4 to 5 Å/min. This is only about 3 times faster than the etch rate of silicon dioxide in EDP, which was measured to be approximately 1.7 Å/min. In the time that is required for EDP etching (generally 2 to 2.5 hours), approximately 700Å of TiN is removed. Providing extra precautions are taken to ensure adequate thickness prior to EDP etching, the use of TiN as a site material would therefore be feasible with respect to process compatibility. The next step will be to fabricate probes using TiN sites and to study their electrical and mechanical properties to determine if indeed they may be a favorable alternative to IrO electrodes.

4. Parylene Coating/Ablation Results on Stimulation Probes

During the past quarter, in a joint experiment with PI Medical of Portland Oregon, we started to develop a process for coating silicon probes with parylene. This post-processing step is of interest to us because of parylene's known protective characteristics, its biocompatablity, and a desire to increase the stiffness of some long probes used for deep structure stimulation. Several acute devices were coated with various thickness of parylene. The sites were then exposed by laser ablation. Electrochemical testing and SEM analysis showed that the many of the sites had not been completely exposed by laser ablation. This affected the electrical characteristics of the electrodes. Additionally, it is suspected that a small amount of parylene remained on the electrodes, further reducing their current carrying ability. Electrochemically cleaning the sites resulted in impedance magnitude's similar to sites on an uncoated probe. Future work is planned to improve this method.

Methods

Two electrode designs were used in this experiment: SX07 and SX04. Both are acute electrodes with large sites. The SX07 has five shanks with one 2000 mm^2 site per shank. The SX04 has one shank with five 4000 mm^2 sites. The probes were mounted on PC stalks in the standard fashion. PI Medical applied the parylene coating to the probes and then used a laser to remove the coating to expose the site. The following details on parylene deposition and laser ablation were supplied by Chris Pogatchnik of PI Medical. The parylene coating was applied with a Labcoter 2010 (Specialty Coating Systems, Indianapolis, IN). The parylene used was parylene C, as opposed to parylene D or parylene N, which are used for microelectronics applications. The probes were coated with parylene in a chemical vapor deposition process. Because parylene does not form a chemical bond with the material it is coating, silane adhesion promoters are sometimes used to promote adhesion between metal and parylene. No adhesion promotion was used with the Michigan probes. There were four coating groups. Parylene films 3, 6, 9, and 12μm thick were deposited.

The laser is an ESI model 4420 (Electro Scientific Industries, Portland OR). Normally, a Nd:YAG laser gives off light at a wavelength of 1064nm, but the wavelength was reduced to 266nm by quadrupling the frequency. The frequency was quadrupled by using two doubling crystals made of Beta Barium Borate (BBO). The UV wavelength is significant because the light-material interaction is photoablative rather than thermal, so

ablation with this laser involves less melting and is a cleaner process. The laser operates in a pulsed mode, typically pulsing at a rate of 1000Hz or within an order of magnitude of 1000Hz. Pulses are 30 to 40 nanoseconds in duration. Laser power is measured with a thermal detector. Average power is at maximum at a laser pulse rate (or rep rate) of 2 kHz, so that is where all power measurements are made. Average laser power can be set from 0 to 300 mW. The objective lens of the laser has a focal length of 25 mm and focuses the spot to approximately 20μm in diameter. The path of the laser is controlled by a beam positioner that can travel to any coordinate in a 3 inch by 3 inch area to within a micron accuracy.

Generally, parylene ablates easily. Unfortunately, removing the last residual layer of any insulator is difficult. This difficulty is usually overcome by hitting the insulator with additional passes. In this case, this is problematic since thin metal layers also ablate easily (discussed later). A proposed solution is to use an oxygen plasma to remove the last bit of parylene to expose the metal. This process will also oxidize iridium, which may be beneficial or detrimental.

Electrochemical Testing

The two probe groups were treated differently in terms of laser ablation. The SX07s were ablated with just enough passes until it appeared (visually) that the parylene had been removed. The SX04s were ablated more aggressively, to ensure the removal of parylene, possibly at the expense of the iridium. To date, only the SX07s have been analyzed completely. The SX04s will be discussed in the next report. Cyclic voltammetry and impedance spectroscopy data were collected for several electrode sites. Initial impedance data of the coated electrodes showed that, despite ablation, the electrodes had a significantly higher impedance (vs. an uncoated probe), both before and after activation (Fig. 2). Activation of an electrode from the 3μm group showed that the coated probes could not achieve the charge storage capacities of an uncoated probe when both were activated (Fig. 3). These initial results suggested that residual parylene was inhibiting electrical conduction at the interface, a possibility noted by PI Medical. It is known that biasing iridium at potentials outside the water window will result in H_2 or O_2 evolution, depending on the polarity of the voltage. The electrode potential was held at -2.5V and then 3V for 3 minutes each. It was hoped that bubbling gas at the sites would clean the electrodes and remove any parylene. Bubbling did result in better oxide formation during activation and, consequently, lower impedance (Figs. 4, 5). It is speculated that gassing cleaned the sites of residual parylene, allowing near normal activation to occur.

SEM

Scanning electron microscopy was used to visualize the sites. Images of the four coating thickness on SX07's are shown in Figs. 6-9. Generally, it appears that the laser can ablate a fairly precise geometry. The 3μm coated probes sites were almost completely exposed (Fig. 7). Probes with 6, 9, and 12μm coatings had a majority of their sites exposed, but a significant portion of the electrode site is covered by thick parylene. This is not a residual layer, but parylene that was purposefully left. No difference was noted visually between sites that had been cleaned with bubbling and those that were untreated. That is, if a residual amount of parylene was causing the increase in impedance, such a layer was not visible with the SEM. More sophisticated surface analysis techniques, such as elemental analysis, may be used in the next quarter to determine the presence of parylene.

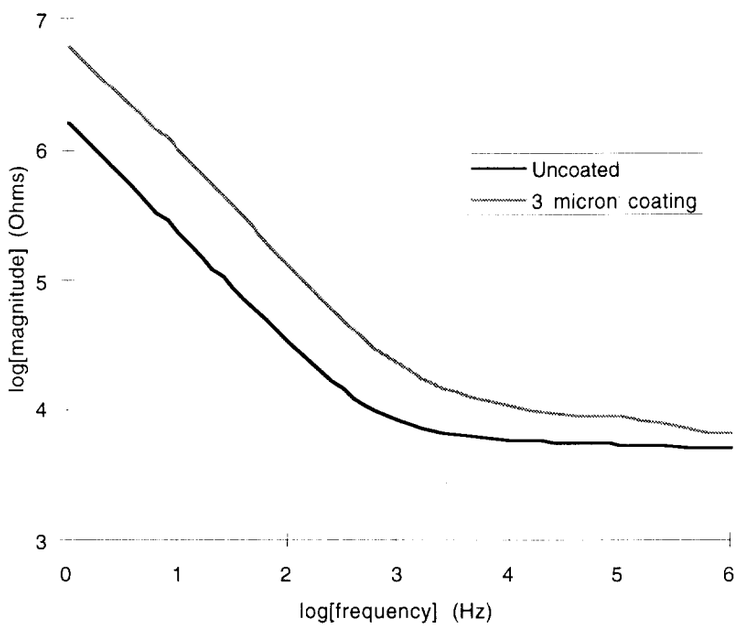

Fig. 2: Impedance magnitude of activated 2000μm^2 electrodes, uncoated and from the 3μm parylene coating group.

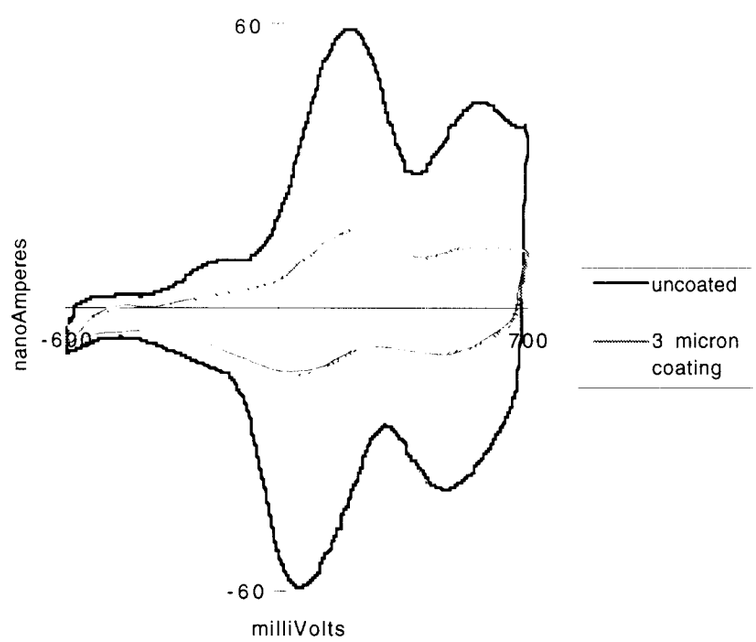

Fig. 3: Cyclic voltammagrams of activated 2000μm^2 electrodes, uncoated and from the 3μm parylene coating group.

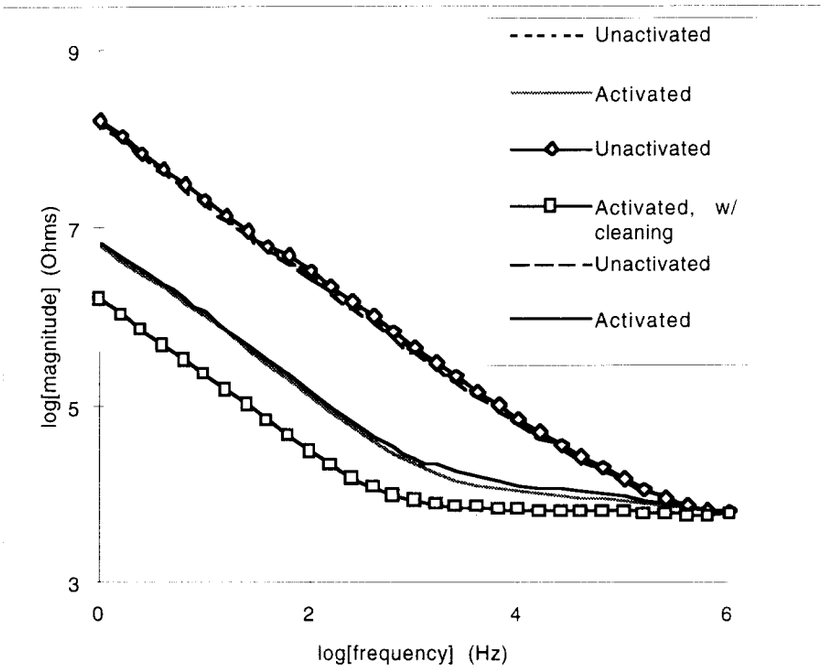

Fig. 4: Impedance magnitude of three 2000μm^2 electrode sites, before and after activation.

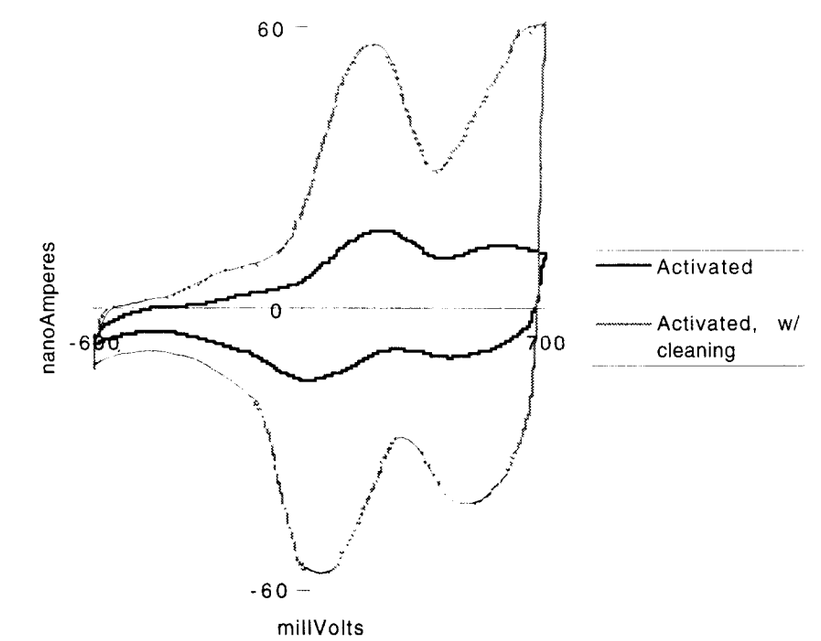

Fig. 5: Cyclic voltammagrams from activated 2000μm^2 sites on an electrode from the 3μm coated probe group.

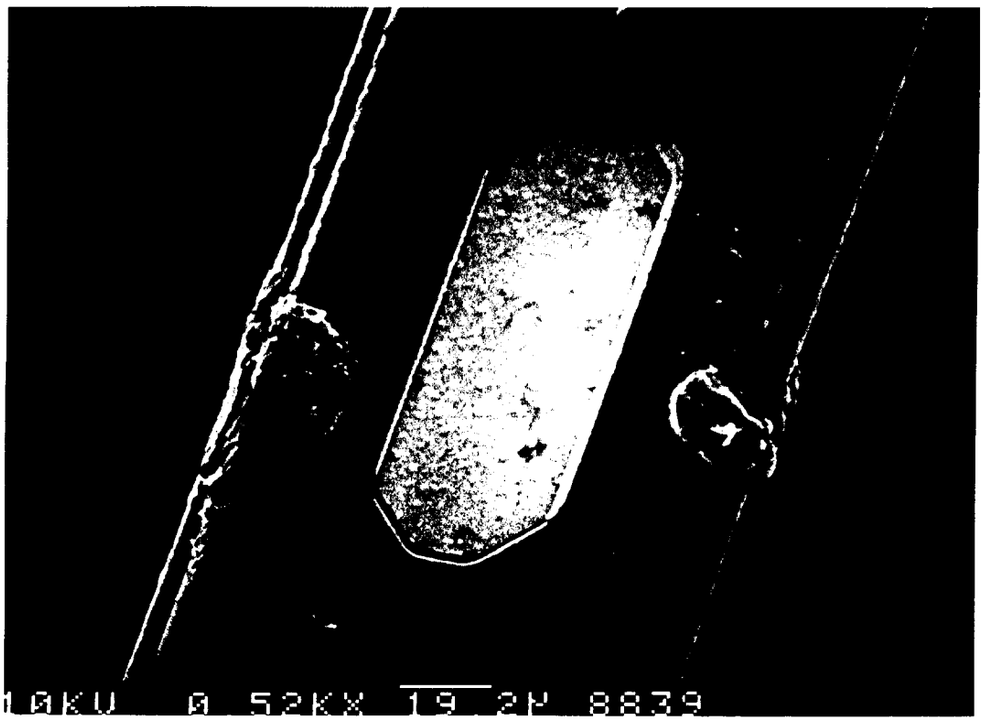

Fig. 6: SEM view of a 2000μm^2 stimulating site covered by a 3μm-thick layer of parylene and laser ablated to expose the site.

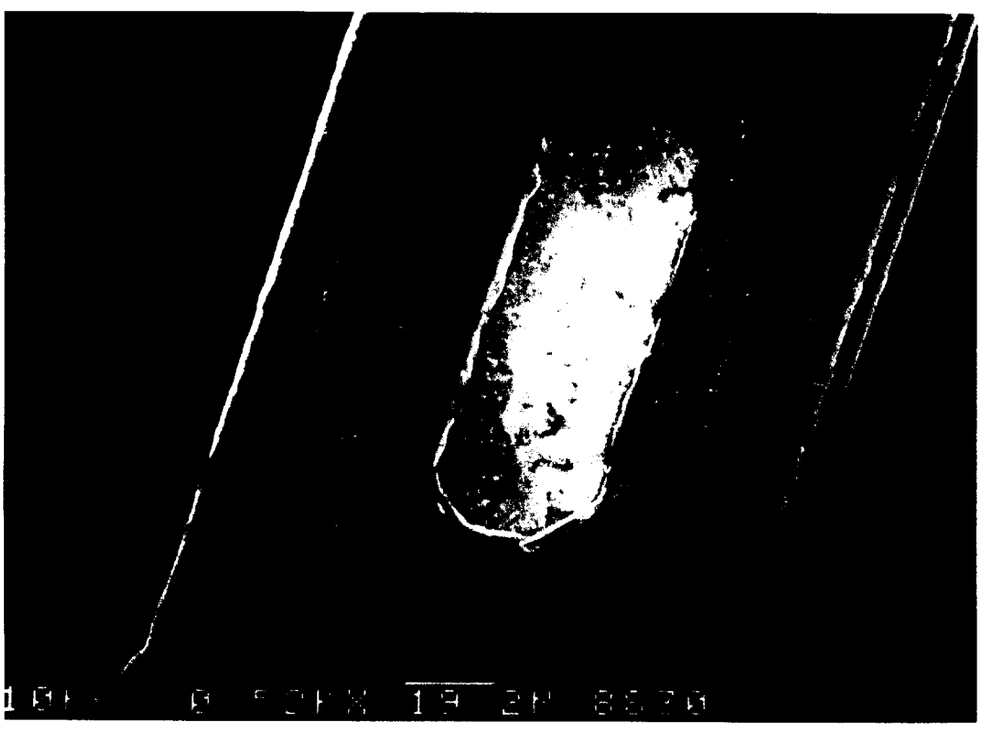

Fig. 7: SEM view of a 2000μm^2 stimulating site covered by a 6μm-thick layer of parylene and laser ablated to expose the site.

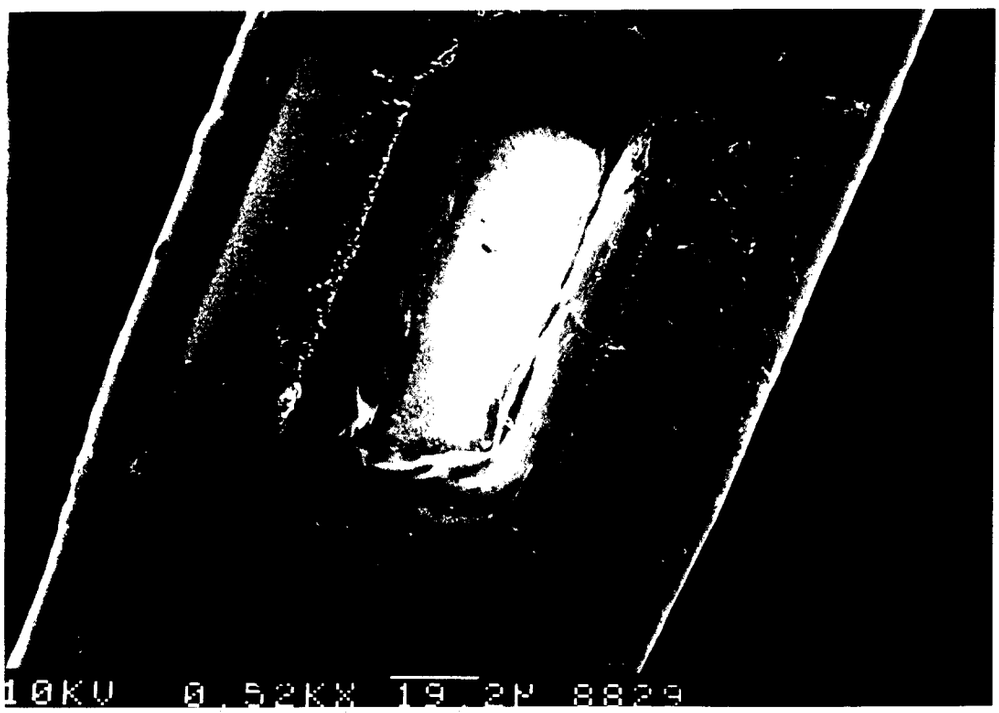

Fig. 8: SEM view of a 2000μm^2 stimulating site covered by a 9μm-thick layer of parylene and laser ablated to expose the site.

Fig. 9: SEM view of a 2000μm^2 stimulating site covered by a 12μm-thick layer of parylene and laser ablated to expose the site.

Another observation was the presence of holes in several of the iridium sites. Apparently, the laser has the power to mill iridium metal. A close up of this is shown in Fig. 10. Holes were seen on 4 of the 20 sites examined. These probably result from exposing the iridium to the laser after most of the parylene has been ablated.

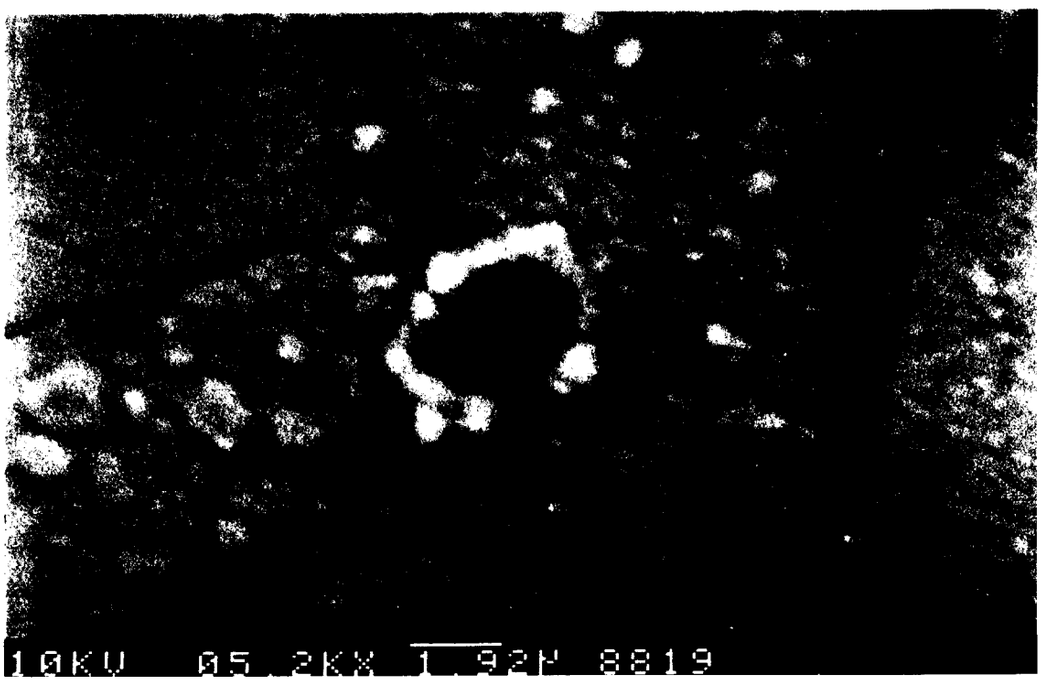

Fig. 10: Close-up of a hole in the 12μm-thick parylene-coated laser ablated site.

Discussion

The impedance of the cleaned sites, activated and unactivated, was dependent on the thickness of the parylene (Fig. 11). High frequency impedance increased with film thickness. Impedance in this region is mostly resistive and can be considered the access resistance seen by a current pulse. It is not clear if the relationship between impedance and film thickness is due to the amount of the site covered by unablated parylene or to the height of the sidewall. Clearly, more exposed site area will lead to lower impedance. However, it has been shown that recessed electrodes will have a higher access resistance, and that the access resistance increases with depth of the recess[2]. Both the sidewall and decreased surface will contribute to the impedance increase. In the next quarter, we hope to test probes with equivalent surface area (i.e., whose sites are exposed completely), but varying coating thickness.

---

[2]Rubenstein, J.T., et.al., "Current Density Profiles of Surface Mounted and Recessed Electrodes for Neural Prostheses", IEEE Trans. on Biomed. Eng., Vol. BME-34, No. 11, Nov. 1987.

The level of charge storage of the electrode (Figs. 12, 13) suggest a smaller electrochemical surface area for the electrodes with 9 and 12μm coatings. Lower charge storage is also evident in the increased low frequency impedance for these coatings. This corresponds to SEMs showing a large portion of the sites for these thicknesses covered by thick parylene On the other hand, the 3μm coated electrode matched the charge storage and impedance of the uncoated electrode at low frequency, which suggests that the site for this coating thickness was completely exposed by ablation and cleaning. The SEM of this site shows that nearly all of this site was indeed exposed by ablation (Fig. 6). The increased high frequency impedance for the 3μm coated probe may be due to the slight recess.

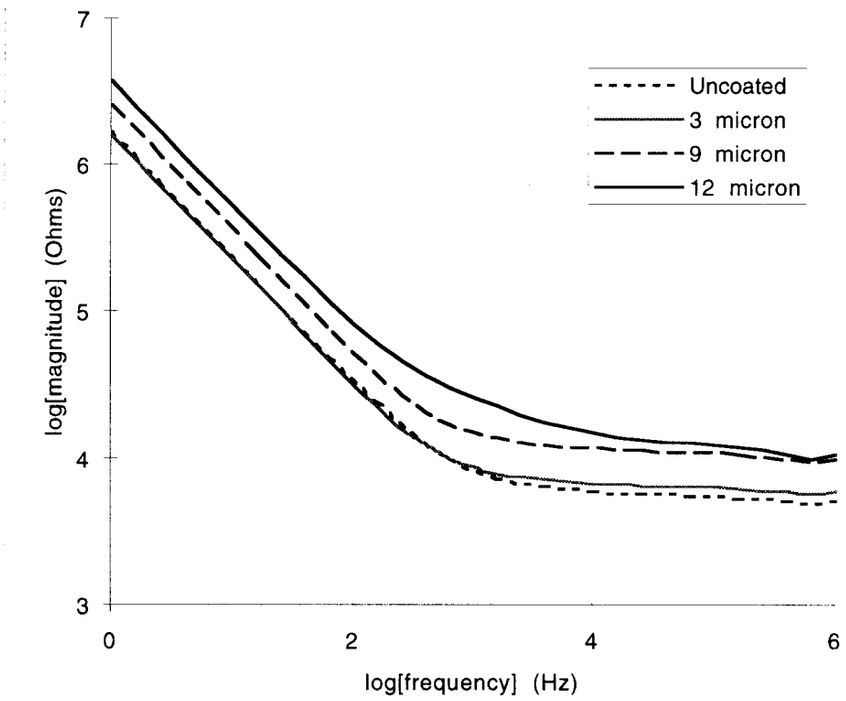

Fig. 11: Impedance magnitude of 2000μm^2 sites for various coating levels, activated with cleaning.

In order to reduce the risk of harming the iridium, a step may be added to the site opening process. The laser will be used to remove most of the parylene above a site, leaving a layer less than a micron thick. Then, an oxygen plasma will be used to etch away the remaining parylene to expose site. This step will also etch parylene covering the rest of the probe, but will not remove enough to significantly effect the mechanical properties of the coating.

The electrical properties of parylene coated probes have been investigated. Acute probes were coated with parylene of varying thickness. The coating over the site was ablated using a laser. Electrochemical cleaning of the electrode surface (i.e., bubbling gas) decreased the impedance of the electrodes. It is theorized that the cleaning process removed a residual layer of parylene.

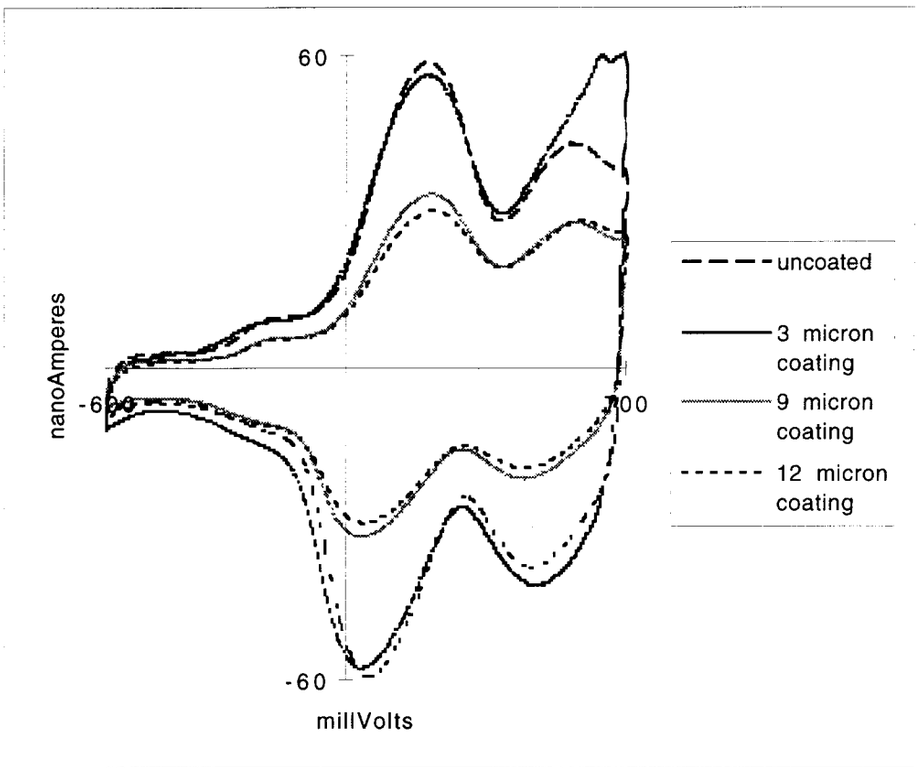

Fig. 12: Cyclic voltammagram of 2000μm^2 sites for various coating levels, activated with cleaning.

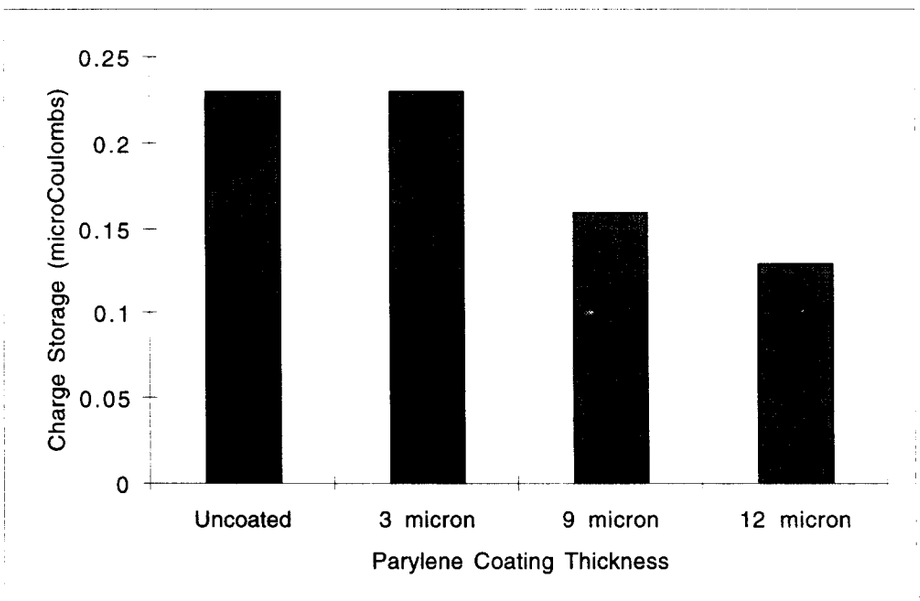

Fig. 13: Charge storage vs. coating thickness

5. *Active Stimulating Probe Development*

During the past quarter, work in the area of the active stimulating probes has concentrated on completing the STIM-2B design, layout and simulation. Also, the possibility of extending the current STIM-2B design to a 3-dimensional array is being explored. Finally, the overall requirements for the 3-dimensional array which will use STIM-2 as the 2-D building block are being developed. The fabrication of a new series of STIM-1A, STIM-1B, and STIM-2 probes has also proceeded and should be completed during the coming term.

STIM-2B

The design and simulation of the second-generation four-channel 64-site version of our monopolar active stimulating probe, STIM-1B, which is identified as STIM-2B, has now been completed. The probe, as shown in the block diagram of Fig. 14, utilizes a 20b shift register to load four 4b site addresses. These addresses are decoded by a 1-of-16 decoder to connect the designated sites to analog input/output pad through large CMOS pass-gate transistors to allow the 'steering' of externally generated currents to the specified sites. The extra fifth bit in each address is included as a flag bit in order to select between the normal stimulating mode and a newly added recording function. The fifth bit simply selects either a direct path between the I/O pad and the site or a path through an amplifier for simple recording from the same site.

The functionality of the probe is quite simple. At power-up, a power-on-reset (POR) circuit initializes all of the circuitry to a startup state which connects all of the sites to the I/O pads to allow parallel activation of all of the iridium sites. After activation, the first clock pulse resets the POR circuitry, which then switches the probe circuitry over to normal operation. The probe can also be initialized via a negative strobe on the clock line. The strobe sets the POR latch to its 'power-up' state where again it remains until a clock pulse resets it. Additional circuitry on the first site allows the site to be de-selected while the clock strobe is held low thus making leakage current measurements very simple to perform. Since the functionality of the probe is almost entirely digital, this design is expected to be highly independent of process variations in the device parameters.

The STIM-2B probe design has been completed and the simulation of each circuit block has demonstrated that they all work as designed. The layout of the circuit blocks has allowed the automatic extraction of circuit parasitics, which were included in the simulation. Because of the mixed tri-level logic nature of the circuitry, all simulations were performed as complete analog simulations at 10MHz. Though we do not anticipate operating the probe at 10 MHz, all circuit blocks were found to function quite well even at such a high frequency. The circuits were also simulated using different process parameters to be sure that they would continue to function normally. All circuits were shown to work for both a 300Å and 500Å gate oxide processes, although, as expected, the speed was degraded for the thicker oxide due to the resulting reduced current drive. Although most of these circuit blocks are fairly standard digital circuits, the functionality of some of them is definitely not standard in that they allow the use of ±5V power supply rails that enable the use of positive and negative drive currents.

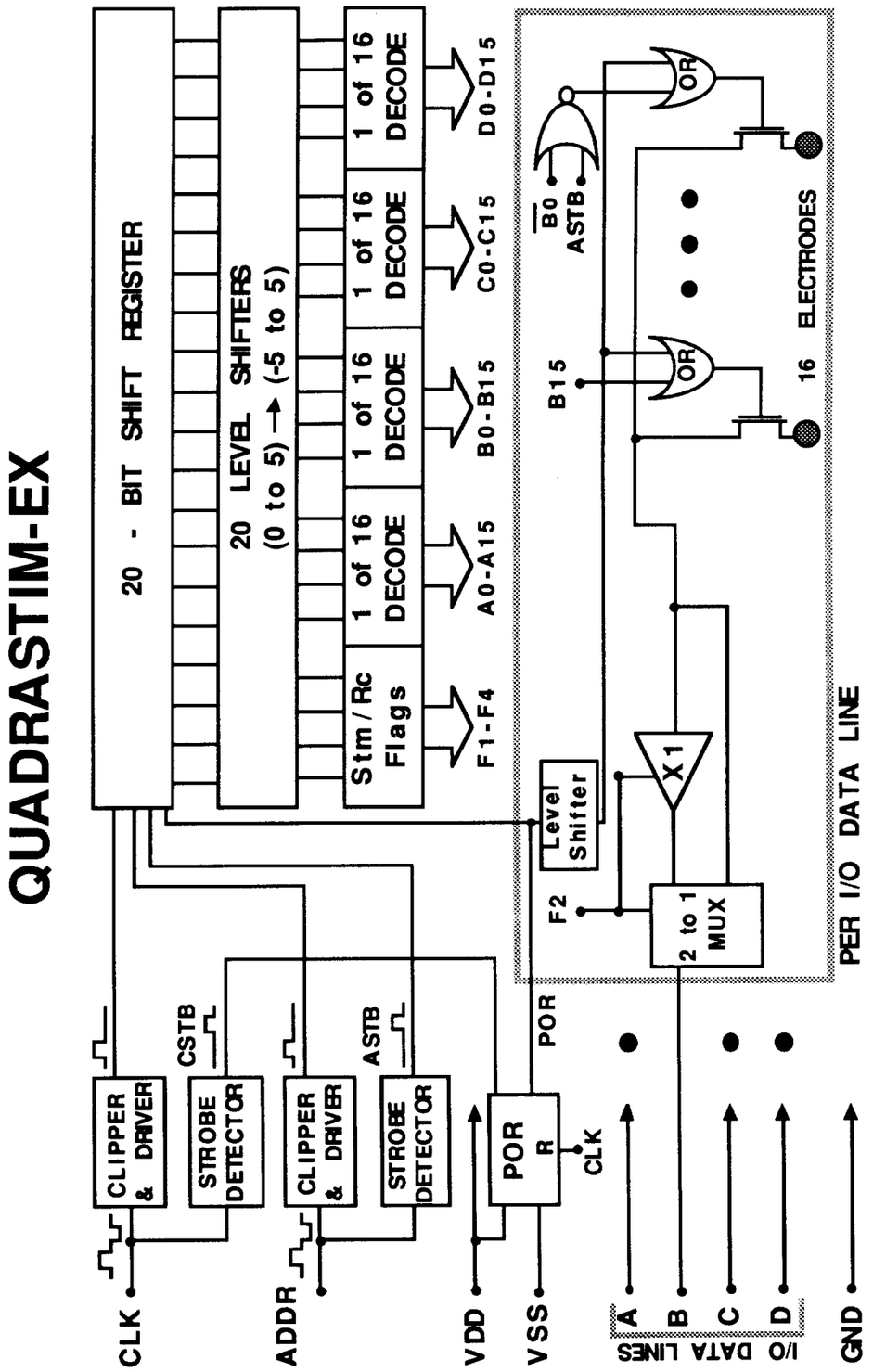

Fig. 14: The overall block diagram of STIM-2B.

Referring to Fig. 14, the serial input shift register uses standard 0-5V logic and each register bit, as shown in Fig. 15, is made up of two six-transistor SRAM cells gated by a two phase clock. The first SRAM includes a reset switch which is used at power-up by the POR to initialize the shift-register. The shift-register functions properly; some of the performance specifications are summarized at the end of this section along with the specifications for the other circuit blocks.

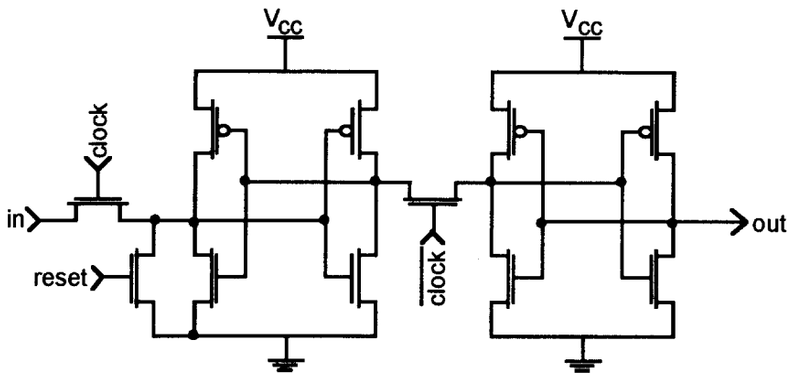

Fig. 15: A single bit of the serial input shift register which also includes a reset switch for state initialization during power-up.

The POR circuit is shown in Fig. 16. The latching nature of the circuit keeps it in the power up state until forced out by a clock pulse. By including a reset switch, the same circuit can be used to re-initialize the probe at any time without cycling the power.

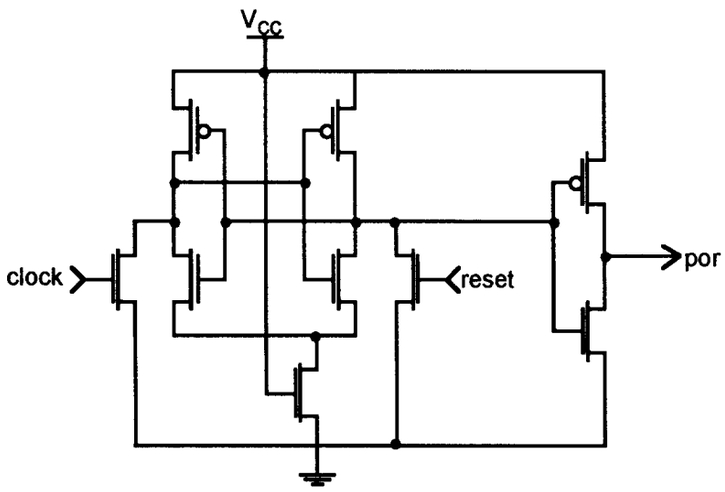

Fig. 16: The power-on-reset circuit for initializing the power-up state of the probe.

The level-shifting circuitry, Fig. 17, is key to the operation of this probe. This circuit converts the normal 0-5V logic to ±5V logic which is required for the operation of the current steering pass gates. The pass gates must function for both positive and negative

voltages, which they will experience during sourcing/sinking of stimulation current. The simulated behavior of the level-shifter is shown in Fig. 18.

The negative strobe detector circuit shown in Fig. 19 is the block of circuitry which senses when the clock line input voltage drops negative and a positive pulse is generated in response. This circuit is used to generate a reset signal for the POR circuitry, which in turn re-initializes the probe to its power-up state. Figure 20 demonstrates the behavior of the strobe detector during positive and negative pulses.

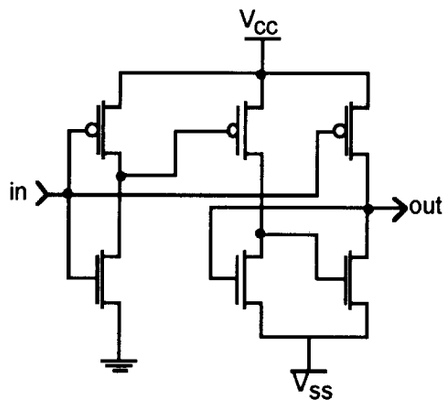

Fig. 17: The level-shifter circuit which converts a standard 0-5V signal to a ±5V signal.

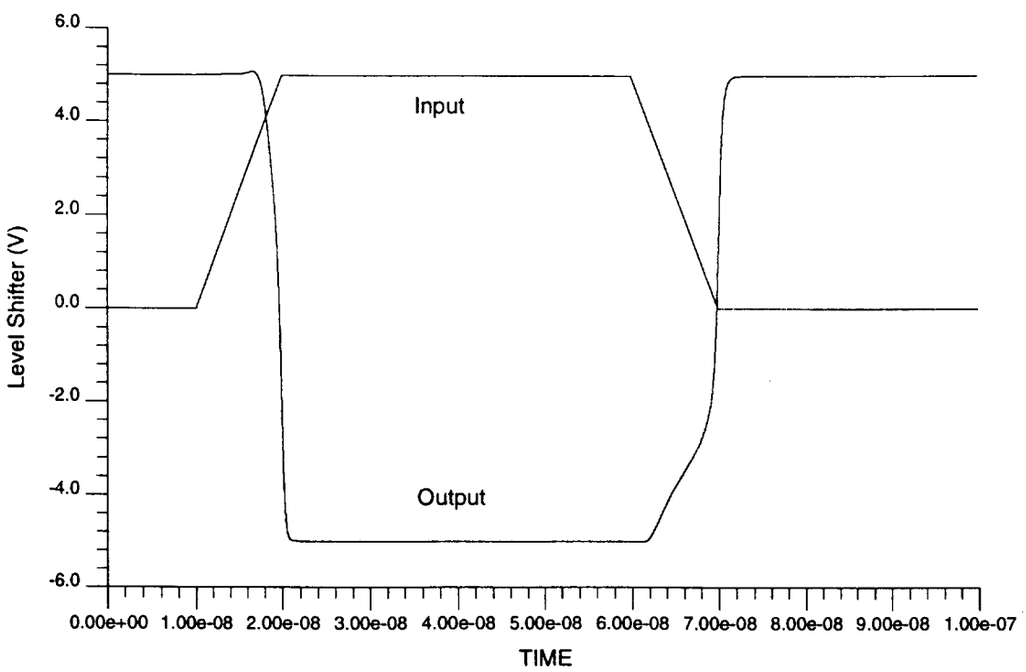

Fig. 18: The response of the level-shifting circuitry to a 5V pulse.

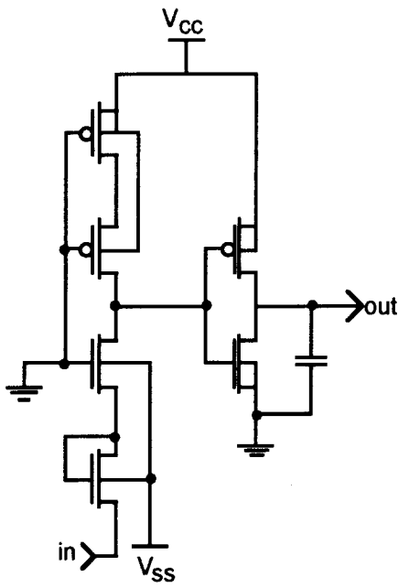

Fig. 19: The negative strobe detector circuit used to detect a negative voltage on the clock line for use in system initialization.

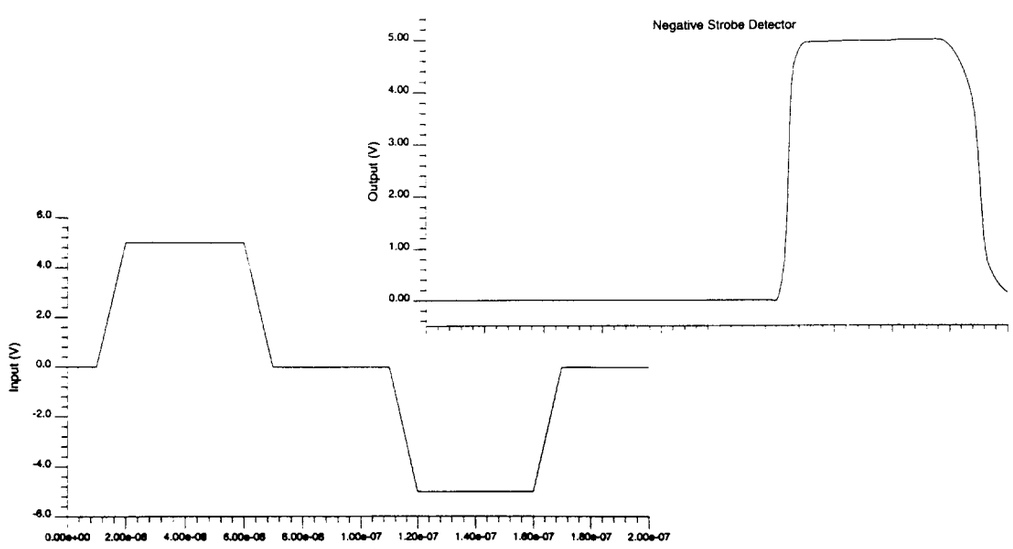

Fig. 20: The simulated behavior of the negative strobe detector in response to a normal positive input pulse and to the negative input pulse.

Simulation of the circuitry demonstrated that all of the circuitry is functioning as designed. The completion of the layout has allowed the extraction of parasitics. The inclusion of these effects in the simulation should have revealed anything that could cause the circuits to behave abnormally, so we feel confident that after fabrication, these probes will function as designed. A summary of some of specifications of the various circuits is included in Table 2 below.

Table 2:

Specification Summary

(All varying inputs have rise and fall times of 10nsec)

POR		
	fall delay	9.57nsec (Input: clk)
	t_f =	1.87nsec (Input: clk)
	rise delay =	5.79nsec (Input: CSTB)
	t_r =	1.57nsec (Input: CSTB)
Strobe Detector		
	rise delay =	9.58nsec
	t_r =	4.12nsec
	fall delay =	25.55nsec
	t_f =	10.27nsec
Shift Register Cell		
	rise delay =	0.92nsec (resetable SRAM)
	fall delay =	1.44nsec (resetable SRAM)
	rise delay =	0.70nsec (SRAM)
	fall delay =	1.70nsec (SRAM)
Level Shifter		
	rise delay =	4.86nsec
	fall delay =	4.70nsec
	t_r =	6.15nsec
	t_f =	1.96nsec
Decoder		
	rise delay =	2.45nsec (input closest to rail switching)
	fall delay =	2.47nsec (input closest to rail switching)
	tr =	3.53nsec (input closest to rail switching)
	tf =	2.74nsec (input closest to rail switching)
Power Passgate		
	rise delay =	2.92nsec (with 5k ohm load)
	fall delay =	10.82nsec (with 5k ohm load)
	Frequency Response: -3dB > 1MHz	
	0.0314V drop @ 200μA	
	0.0409V drop @ -200μA	

Figure 21 shows the overall layout of one version of STIM-2B. The circuit area is about 5.7mm^2, which is about half of STIM-2. With 16 shanks on 400μm centers, the probe is 6.4mm wide. The probe has a height of the probe above the base of the shanks is about 1.8mm, which is higher than we would like for a platform-mounted design. Part of the reason for this height has to do with the front-end connection matrix. In the present design, each of the four input current channels can be routed to each of the four-site shanks. This allows considerable freedom in the current generation patterns that are

possible but requires considerable interconnect area. A simpler interconnect matrix such as that used on STIM-2 would reduce this area considerably and will be reviewed prior to actual mask generation.

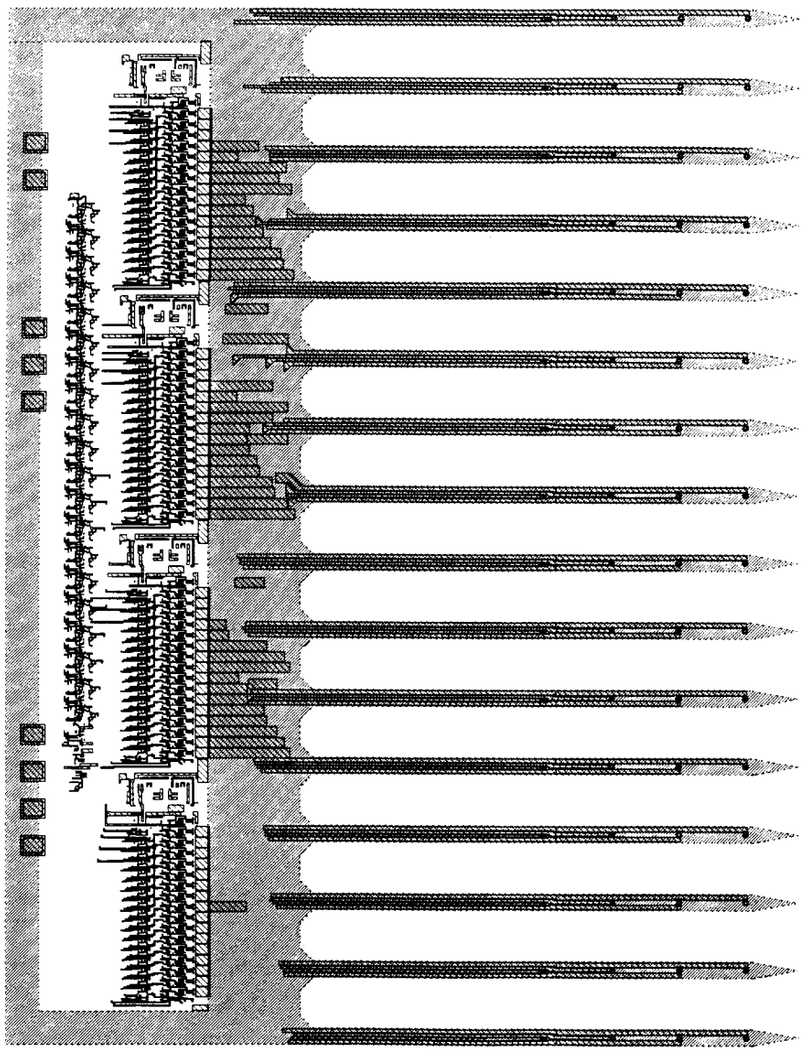

Fig. 21: Layout of a 64-site four-channel active stimulating probe, STIM-2B.

6. *An External Interface to the Active Stimulating Probes*

The design of the new external electronic system is approximately 80% complete, with some redesign required due to updated requirements. The previous system was centered around an 8-bit microprocessor and dual-port RAM acting as a flexible software-programmable sequencer capable of implementing a wide variety of probe communication protocols. With an increased interest in multi-probe stimulation (such as for 3D probe arrays), the issues of data multiplexing and inter-probe synchronization require a more powerful central processor. The 8-bit processor has therefore been replaced with a TMS320C26 Digital Signal Processing (DSP) chip, chosen for its faster execution speed, microcontroller-like features (such as the ability to load code from an external serial port), high-throughput data instructions, and low cost. We believe that this processor will be better able to handle the higher throughput and synchronization tasks that may be required.

Since this processor requires its own RAM, the programmable sequencer will be implemented with a retransmit-capable parallel FIFO instead of a dual-port RAM. Although the number of sequencer steps will now be limited to 128 (the FIFO depth) rather than the 32 Kwords of the dual-port RAM, we believe that this will be sufficient for all foreseeable probe communication protocols. The latest system design is diagrammed in Fig. 22 in block format.

Although the processor block has been changed significantly, the core design of the sequencer and probe drive circuitry are unchanged from the previous design iteration. The schematics for these sections have been captured electronically and are ready for prototype and simulation. We expect to have this activity completed by the end of the quarter, in addition to completing the remaining details and schematic capture of the overall design. Since there are still some unresolved issues regarding the design requirements (for example, in analog current drive capability), the design may have to be amended or augmented as necessary. These additional requirements are not expected to greatly affect the existing design blocks (processor, sequencer, and probe drive circuitry).

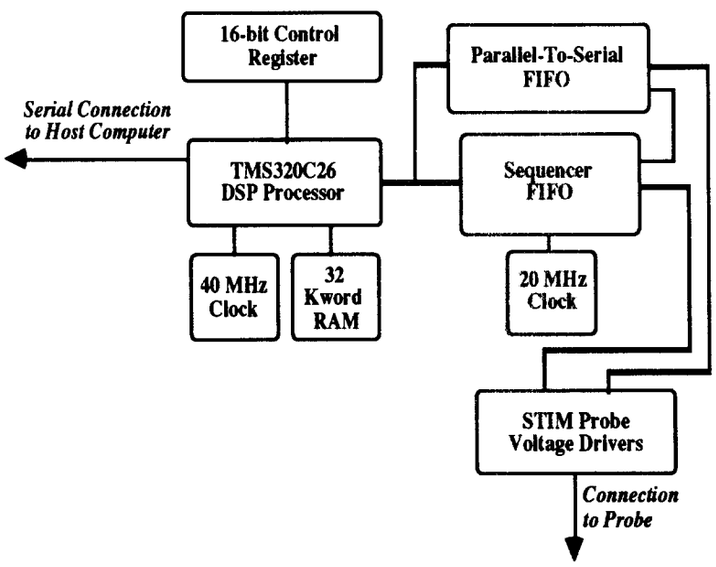

Fig. 22: Block diagram of the new external interface to active stimulating probes.

7. *Conclusions*

During the past quarter, we have continued to fabricate passive stimulating probes and have also realized probes in cooperation with an external foundry (MCNC, Research Triangle Park, NC). The foundry probes use low-stress silicon nitride dielectrics and appear quite acceptable in terms of built-in shank stress, in-vitro tests, and general yield. In-vivo tests are planned during the coming term. We are also beginning work to evaluate the use of TiN layers as an alternative to IrO on some of our stimulating probes. This material does not etch excessively in EDP and is thus compatible with our overall process. It has been reported to have a charge delivery capability significantly better than IrO. We have been using it experimentally under titanium to enhance our circuit contacts, and it is widely known as a passive interdiffusion barrier for contacts in the integrated circuit industry. Probe fabrication using TiN sites will take place during the coming term along with in-vitro and in-vivo evaluation.

We have also begun experiments with parylene as a coating material for some of our stimulating probes. Test probes with parylene coatings 3, 6, 9, and 12μm-thick have been fabricated and the sites have then been laser ablated in cooperation with PI Medical. Some of the sites were then subsequently cleaned electrochemically. The impedances of the sites, activated and unactivated, were dependent on the thickness of the parylene and it is expected that a thin layer of parylene was still present on portions of the metal surfaces after ablation. Use of a post-ablation oxygen plasma to remove the residual parylene will be explored during the coming term.

The design of a four-channel 64-site active stimulating probe has now been completed. This probe has been fully simulated and is functional at clock rates exceeding 10MHz. The circuit layout area is 5.7mm^2. The probe allows each of four externally generated stimulus currents to be routed to 16 sites, with one of the sites on each of the 16 shanks. Any of the selected sites can be used for either recording or stimulation. Fabrication of these probes will also take place during the coming term.